

# Isovector soft dipole mode in ${}^6\text{Be}$

A.S. Fomichev<sup>a</sup>, V. Chudoba<sup>a,b</sup>, I.A. Egorova<sup>c</sup>, S.N. Ershov<sup>c</sup>, M.S. Golovkov<sup>a</sup>, A.V. Gorshkov<sup>a</sup>, V.A. Gorshkov<sup>a</sup>, L.V. Grigorenko<sup>a,d,e</sup>, G. Kamiński<sup>a,f</sup>, S.A. Krupko<sup>a</sup>, I.G. Mukha<sup>d</sup>, Yu.L. Parfenova<sup>a,g</sup>, S.I. Sidorchuk<sup>a</sup>, R.S. Slepnev<sup>a</sup>, L. Standyło<sup>a,h</sup>, S.V. Stepanov<sup>a</sup>, G.M. Ter-Akopian<sup>a</sup>, R. Wolski<sup>a,f</sup>, M.V. Zhukov<sup>i</sup>

<sup>a</sup>Flerov Laboratory of Nuclear Reactions, JINR, Dubna, RU-141980 Russia

<sup>b</sup>Institute of Physics, Silesian University in Opava, Bezručovo nám. 13, 74601 Czech Republic

<sup>c</sup>Bogolyubov Laboratory of Theoretical Physics, JINR, Dubna, RU-141980 Russia

<sup>d</sup>GSI Helmholtzzentrum für Schwerionenforschung, Planckstraße 1, D-64291 Darmstadt, Germany

<sup>e</sup>Russian Research Center “The Kurchatov Institute”, Kurchatov sq. 1, RU-123182 Moscow, Russia

<sup>f</sup>Institute of Nuclear Physics PAN, Radzikowskiego 152, PL-31342 Kraków, Poland

<sup>g</sup>Skobeltsyn Institute of Nuclear Physics, Moscow State University, 119991 Moscow, Russia

<sup>h</sup>Andrzej Sołtan Institute for Nuclear Studies, Hoża 69, PL-00681, Warsaw, Poland

<sup>i</sup>Fundamental Physics, Chalmers University of Technology, S-41296 Göteborg, Sweden

---

## ABSTRACT

By using the  ${}^1\text{H}({}^6\text{Li}, {}^6\text{Be})n$  charge-exchange reaction, continuum states in  ${}^6\text{Be}$  were populated up to  $E_T = 16$  MeV,  $E_T$  being the  ${}^6\text{Be}$  energy above its three-body decay threshold. In kinematically complete measurements performed by detecting  $\alpha+p+p$  coincidences, an  $E_T$  spectrum of high statistics was obtained, containing approximately  $\sim 5 \times 10^6$  events. The spectrum provides detailed correlation information about the well-known  $0^+$  ground state of  ${}^6\text{Be}$  at  $E_T = 1.37$  MeV and its  $2^+$  state at  $E_T = 3.05$  MeV. Moreover, a broad structure extending from 4 to 16 MeV was observed. It contains negative parity states populated by  $\Delta L = 1$  angular momentum transfer without other significant contributions. This structure can be interpreted as a novel phenomenon, i.e. the isovector soft dipole mode associated with the  ${}^6\text{Li}$  ground state. The population of this mode in the charge-exchange reaction is a dominant phenomenon for this reaction, being responsible for about 60% of the cross section obtained in the measured energy range.

*PACS:* 25.70.Kk, 25.70.Pq, 21.60.Gx, 21.10.Sf

*Keywords:*  ${}^6\text{Be}$ , two-proton decay, three-body Coulomb problem, hyperspherical harmonics method, kinematically complete measurements.

---

## 1. Introduction

Electromagnetic excitation is an important tool for studying light exotic (halo) nuclei. Based on the halo hypothesis, the existence of a novel dipole mode at low excitation energies was predicted [1, 2, 3]. This so-called soft dipole mode (SDM) [or soft mode of the giant dipole resonance (GDR)] is related to the low binding energy of the halo nucleon(s). The low binding allows low-frequency oscillations of the halo nucleon(s) against the core, thus creating the low-lying dipole excitations and providing abnormally large cross-sections for electromagnetic dissociation at low-energy. Experiments confirmed these expectations [4, and Refs. therein] and showed that the observed low-lying E1 strength is in a good agreement with the cluster non-energy-weighted sum rule. The latter observation indicates that the SDM is connected with the cluster degrees of freedom in contrast with excitations in

the GDR region, which represent collective phenomena.

The fact that  ${}^6\text{Be}$  is an isobaric partner of the “classical” halo nucleus  ${}^6\text{He}$  is of particular interest to the present work:

- ${}^6\text{Be}$  is the lightest nucleus whose (particle unstable) ground state is a *true two-proton* ( $2p$ ) emitter. True  $2p$  emission is a genuine quantum-mechanical phenomenon, in which due to the pairing effect the emission of one proton is energetically forbidden while the simultaneous emission of two protons is possible. The correlation patterns observed for the decay of  ${}^6\text{Be}$  led to the concept of *democratic decay* [5] which is now generally accepted. In heavier  $2p$ -unstable nuclei the true  $2p$  emission occurs in the form of *two proton radioactivity* [6], as discussed by comparing the correlation data of  ${}^6\text{Be}$  and  ${}^{45}\text{Fe}$  [7].
- Considerable efforts have been made to study the halo

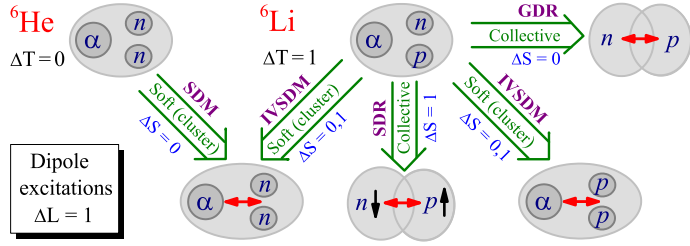


Fig. 1. Classification scheme of dipole excitations in  ${}^6\text{He}$  and  ${}^6\text{Be}$  produced in charge-exchange reactions with  ${}^6\text{Li}$ . The appearance of the soft dipole mode in the *electromagnetic* excitation of  ${}^6\text{He}$  is shown for comparison. Given is the illustration of difference between the cluster excitations (modes), i.e. the soft dipole mode (SDM) and isovector soft dipole mode (IVSDM), and the collective excitations (resonances), i.e. the giant dipole resonance (GDR) and spin-dipole resonance (SDR).

aspect of  ${}^6\text{He}$  in the past two decades. Recently it has been demonstrated in Ref. [ 8] that a valuable alternative to investigating the ground state (g.s.) of  ${}^6\text{He}$  is a precision study of correlations characterizing the decay of the (particle-unstable)  ${}^6\text{Be}$  ground state.

In the present work we studied  ${}^6\text{Be}$  in the charge-exchange reaction  ${}^1\text{H}({}^6\text{Li}, {}^6\text{Be})n$ . We identified the properties of the  ${}^6\text{Be}$  continuum above the highest-lying well-established state, i.e. the  $2^+$  state at  $E_T = 3.03$  MeV,  $E_T$  being the  ${}^6\text{Be}$  energy above its three-body decay threshold. We found that in a broad energy range up to about  $E_T = 16$  MeV this continuum contains mostly negative parity states populated by  $\Delta L = 1$  transitions. The negative-parity continuum in  ${}^6\text{Be}$  can be interpreted to present an analogy to the soft dipole mode in  ${}^6\text{He}$ . Based on the  $\Delta L = 1$  identification in the charge-exchange reaction, it was suggested that the low-energy continuum properties of  ${}^6\text{He}$  [ 9, 10, 11] and  ${}^6\text{Be}$  [ 12] may represent a sort of soft dipole excitation. In this work we are able to confirm this suggestion on the basis of the correlation data. The obtained results provide qualitatively new insight into this problem. We also reveal important differences between our results and data obtained for the SDM in  ${}^6\text{He}$ , which enables us to interpret the continuum structure of  ${}^6\text{Be}$  as the manifestation of a novel phenomenon, namely the isovector soft dipole mode (IVSDM).

The classification of the dipole excitations in  ${}^6\text{He}$  and  ${}^6\text{Be}$  built on  ${}^6\text{Li}$  g.s. is illustrated in Fig. 1. This figure allows to clarify the difference with the interpretation of the dipole excitations in Refs. [ 12, 10, 11] as a part of the GDR or SDR which are collective phenomena. In contrast, our interpretation of the soft dipole excitations in  ${}^6\text{He}$  and  ${}^6\text{Be}$  is entirely connected to the cluster degrees of freedom. We presume that collective resonances are excluded below the  $\alpha$ -cluster disintegration energy and that the observed spectra are thus connected solely with the specific three-body cluster dynamics of  $A = 6$  nuclei. From theoretical arguments there are no low-lying  $T = 1$  resonances of negative parity (structures with definite energy and width) expected in  $A = 6$  nuclei. Therefore, the strong population of the continuum structure in  ${}^6\text{Be}$  has to be interpreted in terms of *excitation modes* which strongly depend on the excitation mechanism.

## 2. Experiment

A 47 A MeV  ${}^6\text{Li}$  beam was produced at the U-400M Cyclotron of the Flerov Laboratory (JINR, Dubna, Russia [ 13]). The fragment separator ACCULINNA [ 14] served as

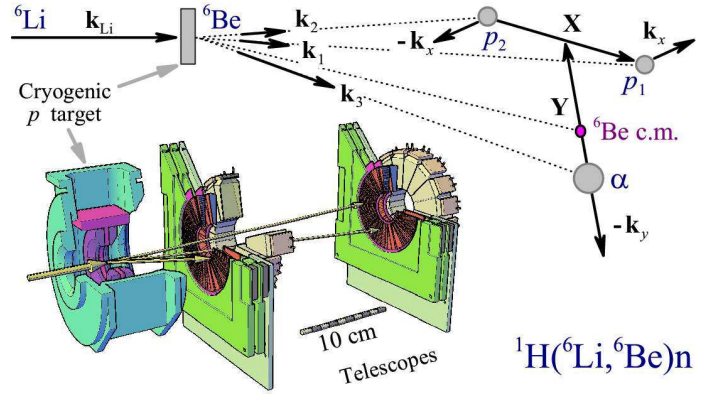


Fig. 2. Experimental setup and kinematical diagram. The coordinate space Jacobi variables  $\mathbf{X}$  and  $\mathbf{Y}$  as well as the conjugated momentum space Jacobi variables  $\mathbf{k}_x$  and  $\mathbf{k}_y$  are shown for the “T” Jacobi system.

a transport line delivering the beam to the target position. A graphite degrader installed in front of ACCULINNA reduced the beam energy to 32.5 A MeV. The beam delivered to the target had an intensity of  $3 \times 10^7 \text{ s}^{-1}$ , an energy spread smaller than 0.5% and covered a circular area of 6 mm diameter.

A schematic view of the experimental setup, the kinematical diagram and the kinematical variables are shown in Fig. 2. The 6 mm thick target cell having 6  $\mu\text{m}$  stainless-steel windows was filled with hydrogen at a pressure of 3 bar and cooled down to 35 K. The reaction products were detected by two identical annular telescopes placed 91 and 300 mm downstream of the target. Each telescope consisted of two position-sensitive silicon detectors of 300 and 1000  $\mu\text{m}$  thickness, respectively, and an array of 16 trapezoidal CsI(Tl) crystals with PIN-diode readouts. The inner and outer diameters of the active zone of the silicon detectors were 32 and 82 mm, respectively. The first detector was segmented in 32 rings on one side and 32 sectors on the other, whereas the second detector had 16 sectors only. The 19 mm thick CsI(Tl) crystals were assembled in a ring with an inner and outer diameter of 37 and 90 mm, respectively. Angular ranges of approximately 3 to 8° and 10 to 24° were covered by the first and the second telescopes, respectively. Each segment of the telescopes had its own acquisition channel. Particle identification was provided by the standard  $\Delta E$ - $E$  method.

## 3. Experimental results

By analysing triple ( $p+p+\alpha$ ) coincidence events, we determined the invariant mass of  ${}^6\text{Be}$  and its center-of-mass (c.m.) momentum vector. Due to the inverse kinematics of the  ${}^1\text{H}({}^6\text{Li}, {}^6\text{Be})n$  reaction the decay products of  ${}^6\text{Be}$  move in forward direction within a rather narrow angular cone. Therefore the two protons and the  $\alpha$ -particle, ejected from the  ${}^6\text{Be}$  continuum states with energies up to  $E_T = 16$  MeV, were detected with reasonable efficiency almost in the whole angular range of  $0^\circ < \theta_{\text{Be}} < 180^\circ$ . The angle  $\theta_{\text{Be}}$  is the  ${}^6\text{Be}$  emission angle which is defined in the c.m. system of the  ${}^1\text{H}({}^6\text{Li}, {}^6\text{Be})n$  reaction. The spectrum measured in this angular range is displayed in Fig. 3 (a). Due to the high statistics, obtained by accumulating approximately  $\sim 5 \times 10^6$   $2p$ -decay events, statistical experimental uncertainties are not visible in Fig. 3 (a). The  $0^+$  g.s. at  $E_T = 1.37$  MeV and the first excited  $2^+$  state at  $E_T = 3.05$  MeV are identified directly in this inclusive spectrum. In the measured spectrum, these

two peaks are superimposed on a broad hump which starts (presumably) from the g.s. energy and has a maximum at  $E_T \sim 6$  MeV. The high-energy slope of the hump is mainly connected to the limited angular acceptance of the detector array and to the decrease of the detection efficiency for protons with laboratory energies above 45 MeV.

The width of the g.s. peak corresponds to the overall energy resolution of the experiment. The energy resolution obtained by Monte-Carlo (MC) simulations can be approximated to follow a  $\sqrt{E_T}$  dependence, resulting in FWHM values of 0.4, 0.6, 1.0 and 1.3 MeV for  $E_T$  values of 1.4, 3, 9, and 15 MeV, respectively.

The two-dimensional plot  $E_T$  vs.  $\theta_{Be}$  based on the measured data and presented in Fig. 3 (c), reveals that the broad hump extending to 16 MeV is characterized by a regular behavior in the whole angular range. As will be discussed in Sec. 5, the events found in any part of this hump show similar regularities both in the angular distribution and in the correlations of the kinematical variables characterizing the three-body decay of  ${}^6\text{Be}$ .

The population of the  ${}^6\text{Be}$  g.s. in the  ${}^1\text{H}({}^6\text{Li}, {}^6\text{Be})n$  charge-exchange reaction is associated mainly with the  $\Delta L = 0$  orbital momentum transfer, providing the cross-section maximum at zero degree. In the experimental spectrum shown in Fig. 3 (c) this maximum is suppressed by the low efficiency for events with small decay energy  $E_T$  and emission angle  $\theta_{Be}$  approaching zero degree. This is caused by the central hole of the second telescope (see Fig. 2) which, however, affects only the low-energy part of the  ${}^6\text{Be}$  spectrum obtained at forward angles and does not significantly distort the rest of the spectrum.

The  $2^+$  excited state of  ${}^6\text{Be}$  is mainly populated by  $\Delta L = 2$  momentum transfer. As can be seen from Fig. 3 (c), the maximum in the angular distribution obtained for this state is located at  $\theta_{Be} = 50^\circ - 70^\circ$ , whereas the maximum of the broad hump above the  $2^+$  state occurs at about  $\theta_{Be} = 35^\circ$ , hence at a much smaller angle than that for the maximum of the  $2^+$  state. This observation suggests that the entire hump structure is related to  $\Delta L = 1$  transfer populating negative parity states with  $J^- = \{0^-, 1^-, 2^-\}$ . To extract more detailed information on this phenomenon the rich data set obtained in the experiment was analyzed by taking into account distortions caused by the detector array. This task can be performed by using a Monte Carlo simulations, provided a proper theoretical model is applied (see Sec. 4).

#### 4. Theoretical model

For the theoretical interpretation of the measured spectra, we extend the approach of Ref. [8] and combine the three-body dynamics for the decay of the  ${}^6\text{Be}$  states with a simple treatment of the reaction mechanism. The properties of the  ${}^6\text{Be}$  continuum is approximated by a three-body  $\alpha + N + N$  wave function (WF) with outgoing asymptotics

$$(\hat{H}_3 - E_T)\Psi_3^{JM(+)} = \hat{O}\Psi_{\text{gs}}^{J'M'} \quad (1)$$

The SDM  $J^\pi = 1^-$  continuum in  ${}^6\text{He}$  is assumed to be populated in electromagnetic transitions by

$$\Psi_{\text{gs}} \rightarrow \Psi_{{}^6\text{He}}, \quad \hat{O} \sim \sum_i Z_i r_i Y_{1m}(\hat{\mathbf{r}}_i), \quad (2)$$

where the index  $i$  indicates the constituents which are the  $\alpha$ -core and the two valence nucleons. For the population

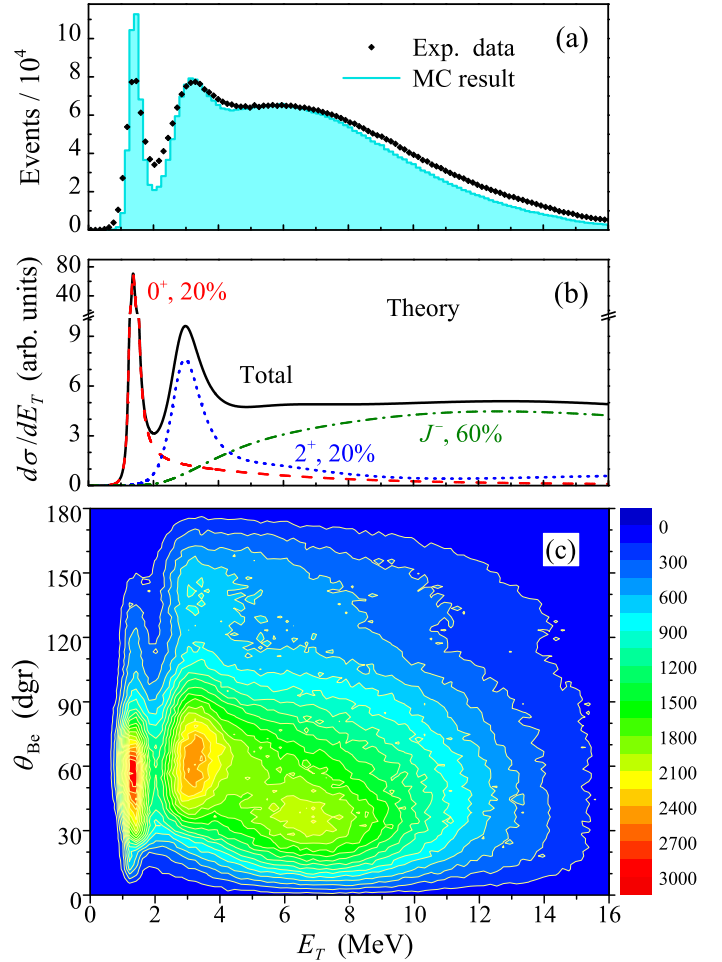


Fig. 3. (a) Experimental energy spectrum of  ${}^6\text{Be}$  (diamonds) and Monte Carlo simulation (shaded histogram). The energy bin size is 140 keV. (b) Spectrum obtained by correcting the experimental data for efficiency, which represents the input for Monte Carlo simulation; the contributions of different  $J^\pi$  components is indicated. (c) Contour plot of the spectrum in the  $\{E_T, \theta_{Be}\}$  plane.

of low-lying states in  ${}^6\text{He}$  and  ${}^6\text{Be}$  in the charge-exchange reaction with  ${}^6\text{Li}$ , the general form of the transition operator is given by

$$\Psi_{\text{gs}} \rightarrow \Psi_{{}^6\text{Li}}, \quad \hat{O} \sim \sum_i f_l(q, r_i) \left[ \alpha + \beta \sigma_\mu^{(i)} \right] \tau_\pm^{(i)} Y_{lm}(\hat{\mathbf{r}}_i), \quad (3)$$

where the index  $i$  indicates the two valence nucleons. The operators  $\tau_-$  and  $\tau_+$  describe the population of the  ${}^6\text{Be}$  and  ${}^6\text{He}$  spectra, respectively. Using the effective spin-spin charge-exchange interaction between the projectile and target nucleons

$$V(r) = V_0(\sigma^{(1)} \cdot \sigma^{(2)})(\tau^{(1)} \cdot \tau^{(2)}) \exp[-(r/r_0)^2],$$

$f_l(q, r_i)$  can be obtained in the plane-wave impulse approximation (PWIA) to be

$$f_l(q, r_i) = V_0 r_0^3 \sqrt{2} \pi^2 \exp[-(qr_0/2)^2] j_l(qr_i).$$

Such a simple choice allows one to reproduce qualitatively well the angular distributions obtained for  ${}^6\text{Be}$ .

The three-body cluster model [15], developed for the  $A = 6$  isobaric chain, was applied to calculate the g.s. wave-function  $\Psi_{\text{gs}}$ . The method, which was successfully applied in Ref. [7] to the studies of the  $0^+$  state, was used for the resonant  $0^+$  and  $2^+$  states. The calculated cross section profiles

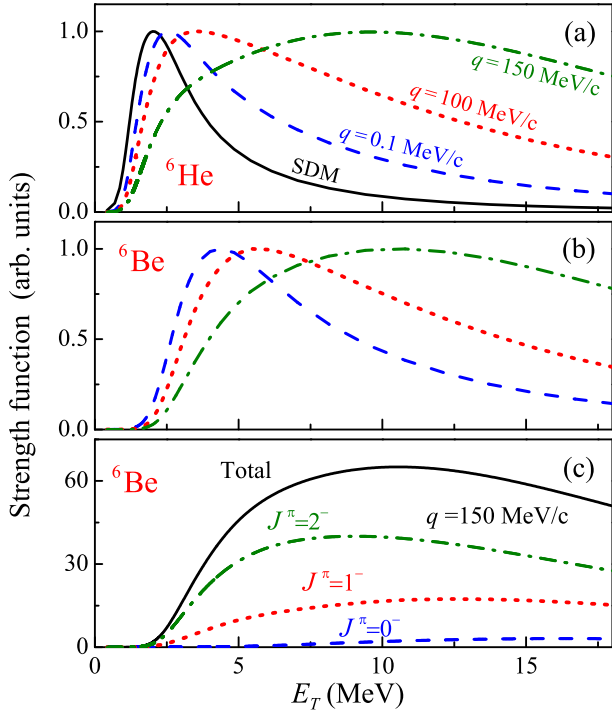


Fig. 4. Theoretical results for negative parity states. (a) The SDM strength function  $dB_{E1}/dE_T$  (solid line) and the IVSDM spectra ( $d\sigma/dE_T$  value) for different transferred momentum  $q$  values in  $^6\text{He}$ . (b) The IVSDM ( $d\sigma/dE_T$  value) spectra in  $^6\text{Be}$ . The meanings of the curves is the same as in panel (a). All curves are normalized to the unity maximum value. Panel (c) shows the contributions of different  $J$  values in one selected ( $q = 150$  MeV/c) IVSDM spectrum of  $^6\text{Be}$ .

are shown in Fig. 3 (b). The cross-section ratios are obtained by fitting procedures, as will be discussed in Section 6.

The continuum wave-function of negative parity states were obtained by using the Greens function method [16]

$$\Psi_3^{JM(+)} = \hat{G}_{3E_T}^{(+)} \hat{O} \Psi_{gs}^{J'M'}, \quad (4)$$

where the exact Greens function of a simplified three-body Hamiltonian is used which is available in compact analytical form:

$$\hat{G}_{3E}^{(+)}(\mathbf{X}\mathbf{Y}, \mathbf{X}'\mathbf{Y}') = \frac{E}{2\pi i} \int_0^1 d\varepsilon \hat{G}_{\varepsilon E}^{(+)}(\mathbf{X}, \mathbf{X}') \hat{G}_{(1-\varepsilon)E}^{(+)}(\mathbf{Y}, \mathbf{Y}'). \quad (5)$$

The vectors  $\mathbf{X}$  and  $\mathbf{Y}$  are the Jacobi variables for the “Y” system:  $\mathbf{X}$  connects the core with one of the valence nucleons, while  $\mathbf{Y}$  connects the second nucleon with the center of mass of the remnant. The operator  $\hat{G}_E^{(+)}$  is an ordinary two-body Greens function. This method takes into account exactly one final-state interaction out of the three ones being present. This was shown to be a good approximation in the case of SDM [16, 17], where the dynamics is defined predominantly by one resonant subsystem (for  $A=6$  nuclei this is evidently the  $p_{3/2}$  resonance in the  $\alpha$ - $N$  subsystem). An analogous approximation has been used in Ref. [18] for the SDM studies in  $^{11}\text{Li}$ .

Figures 4 (a,b) show the comparison of the strength functions for the SDM in  $^6\text{He}$ , see Eq. (2), and the IVSDM in  $^6\text{He}$  and  $^6\text{Be}$  built on  $^6\text{Li}$ , see Eq. (3). As can be seen from Fig. 4, the peak of the IVSDM of  $^6\text{He}$  for small  $q$  values occurs close to that of the SDM but is much broader. This is a consequence of the more compact g.s. wave-function of  $^6\text{Li}$

as compared to  $^6\text{He}$ . However, the steep rise of the spectra occurs in the case of the  $^6\text{He}$  IVSDM at energy 1 – 2 MeV comparable with the SDM case. As can be seen from Fig. 4 (b), the low-energy slope of the IVSDM in isobaric mirror partner of  $^6\text{He}$  (namely  $^6\text{Be}$ ) appear to be at higher energies of 2 – 4 MeV. The theoretical IVSDM curves for  $q = 150$  and  $q = 100$  MeV/c, are displayed in Fig. 4 (b) for  $^6\text{Be}$ . These  $q$  values correspond to c.m. angles of about  $\sim 45^\circ$  and  $\sim 28^\circ$  where the experimental IVSDM peak is located, see Fig. 3 (c). Thus  $q \sim 100 - 150$  MeV/c is a typical momentum transfer for the IVSDM peak. Calculations for  $q = 0.1$  MeV/c can be considered to represent the “long-wave limit”. In this case the transition operator approximately behaves like  $\sim r_i$  providing the dynamical analogue of SDM calculations. The “long-wave” and “short-wave” responses have quite different shapes. However, the phenomenon has stable features with respect to assumptions concerning the source term (reaction mechanism). For example, the strength functions rise practically at the same energy. One can also see that the IVSDM contributes already at the energy of the  $2^+$  state, i.e. around 3 MeV.

Figure 4 (c) shows the population of different  $J^-$  states in our model. The populations of  $2^-$  and  $1^-$  dominate whereas the contribution of  $0^-$  is weak. On the one hand, the presence of states with negative parity but with different  $J$  values makes the picture more complex than in the case of the SDM in  $^6\text{He}$ , where only the  $J^\pi = 1^-$  state is believed to be populated in the Coulomb excitation. On the other hand, the IVSDM provides access to a wider range of dynamical phenomena which can represent an important feature of such studies.

## 5. Data analysis: correlations in $^6\text{Be}$

Without taking the initial orientation into account, the energy-angle correlations of the fragments in the  $^6\text{Be}$  c.m. (so-called “internal” three-body correlations) can be described in terms of the energy distribution parameter  $\varepsilon$  and the angle  $\theta_k$  between the Jacobi momenta  $\mathbf{k}_x, \mathbf{k}_y$ ,

$$\begin{aligned} \varepsilon &= E_x/E_T, \quad \cos(\theta_k) = (\mathbf{k}_x \cdot \mathbf{k}_y)/(k_x k_y), \\ E_T &= E_x + E_y = k_x^2/2M_x + k_y^2/2M_y, \\ \mathbf{k}_x &= \frac{A_2 \mathbf{k}_1 - A_1 \mathbf{k}_2}{A_1 + A_2}, \quad \mathbf{k}_y = \frac{A_3(\mathbf{k}_1 + \mathbf{k}_2) - (A_1 + A_2)\mathbf{k}_3}{A_1 + A_2 + A_3}, \end{aligned} \quad (6)$$

where  $M_x$  and  $M_y$  are the reduced masses of the  $M_x$  and  $M_y$  subsystems (see, e.g., Ref. [8] for details).

To compare the model calculations with the experimental results we made two additional assumptions, namely we neglected the spin alignment of  $^6\text{Be}$  and interference effects. The upper row of Fig. 5 shows the energy-angle correlations obtained for  $^6\text{Be}$  decay products. The correlation plots are built in the “T” system from the experimental data taken in four different ranges of  $E_T$ . The first column of Fig. 5 corresponds to the g.s. population in  $^6\text{Be}$ , the second column shows the correlations obtained in the energy range where the first excited  $2^+$  state has maximal cross section, and the last two columns display similar correlations revealed for  $E_T$  ranging from 5 to 7 MeV and 9 to 11 MeV, respectively, where the population of negative-parity states dominates. The lowest row in Fig. 5 shows theoretical calculations for the energy-angle correlations obtained in the same energy regions. The middle row shows the results of Monte Carlo



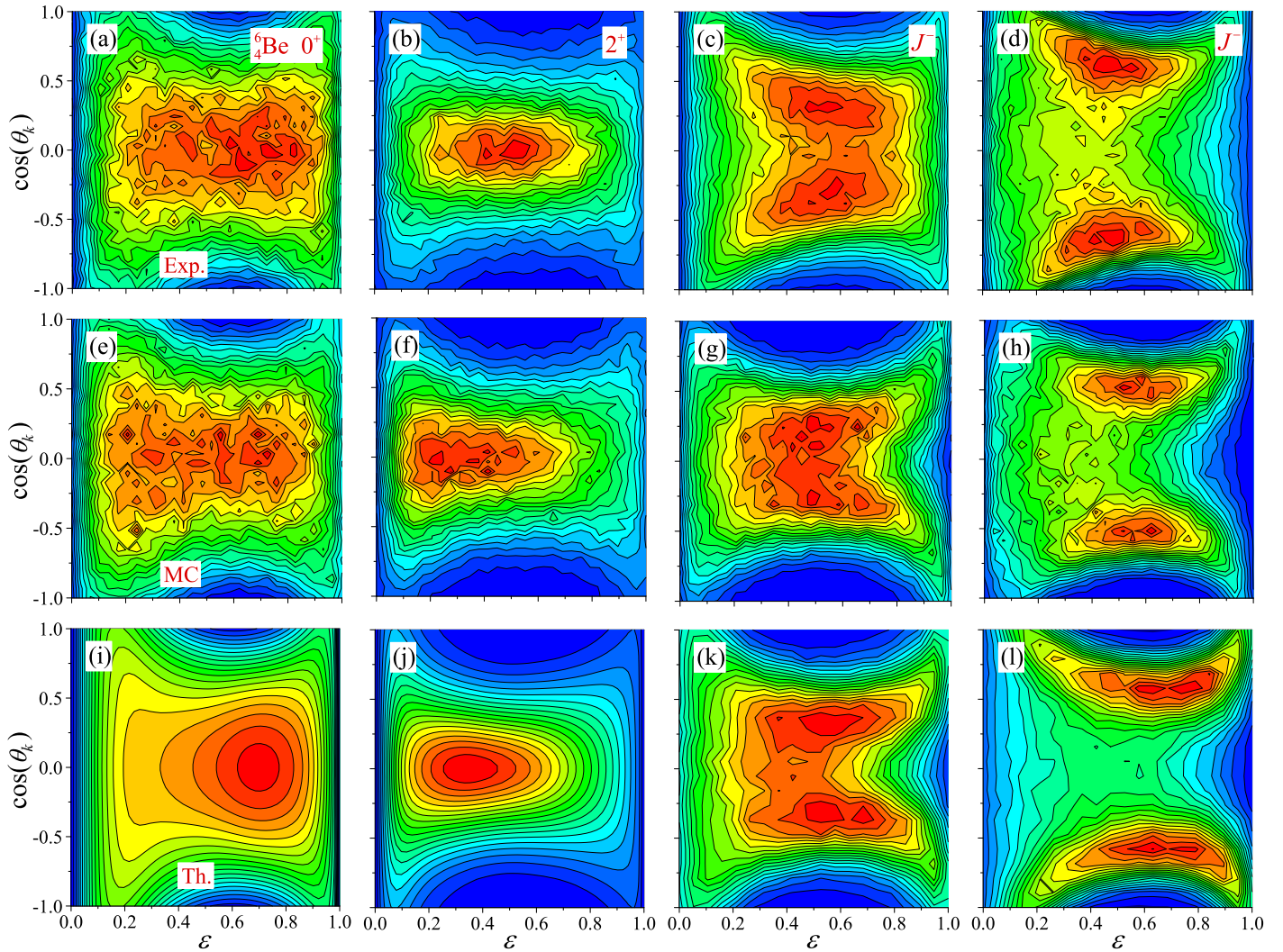


Fig. 5. Internal energy-angle correlations for different states of  ${}^6\text{Be}$  are presented in Jacobi “T” system. Compared are the experimental (upper row), Monte Carlo (middle row) and theoretical (lower row) correlation patterns. Results are presented for the resonant  $0^+$  (a,e,i) and  $2^+$  (b,f,j) states. The  $J^-$  configurations of the IVSDM are given for two energy ranges, namely 5 to 7 MeV (c,g,k) and 9 to 11 MeV (d,h,l). The kinematical variables are defined in Eq. (6).

simulations which were performed in order to correct the theoretical calculations for the instrumental bias. This row can be compared with the upper one where the experimental results are displayed.

Correlations similar to those presented for the  ${}^6\text{Be}$  g.s. in the first column of Fig. 5 were studied in detail in Refs. [7, 8], where the experimental data were well reproduced by theoretical calculations. Our experimental data for the  $0^+$  state also yield full agreement with the model calculations and thus with the data of Ref. [8]. In the present work, high quality energy-angle correlation data were obtained for the  $2^+$  state of  ${}^6\text{Be}$  for the first time. The data deduced for the  $2^+$  state are qualitatively different from those measured for the  $0^+$  state: the profile of the  $\cos(\theta_k)$  distribution is much more narrow for the  $2^+$  state, and the maximum of the correlation distribution is shifted towards smaller relative proton energy. The former observation is consistent with the predictions made for the “democratic” decays in Ref. [19]. The sensitivity of the three-body correlations to the underlying nuclear structure indicates that they may represent a tool for spin-parity identification. The properties of the  $2^+$  state will be discussed to more detail in a forthcoming publication.

The correlations of the broad hump at  $E_T > 4$  MeV are

qualitatively different from the correlations of the  $0^+$  and  $2^+$  state. Correlations found for (tentatively assigned)  $J^-$  states show a smooth dependence on the  ${}^6\text{Be}$  energy but almost none on the c.m. angle  $\theta_{\text{Be}}$ . The pronounced crescent-like ridges exhibited in columns 3 and 4 of Fig. 5 are connected to the  $p_{3/2}$  and  $p_{1/2}$  resonant final state interactions in the core- $p$  subsystem. The evolution of these ridges with increasing  $E_T$  is well described under the assumption of the IVSDM. Comparing the first and second rows in Fig. 5 one can see some differences in details which, most probably, can be explained by interference effects. We leave this problem for a further analysis but emphasize the overall agreement between model calculations and experimental correlations.

## 6. Data analysis: angular distributions and partial cross sections

In order to analyse the angular distributions and the partial cross-sections, the data displayed in Fig. 3 (c) were divided into narrow angular intervals and projected on the energy axis. By using the theoretically predicted energy profiles of the partial cross sections for different  $J^\pi$  values, the experimental data were fitted for each angular interval, yielding the angular distributions for individual  $J^\pi$  contributions.

The  $q$  dependence of the partial cross sections was neglected, and the cross sections were calculated by using the  $q$  values defined for each  $J^\pi$  by the maximum in the angular distribution. Nevertheless, performing Monte Carlo simulations based on the results obtained by the theoretical model, we are able to well reproduce the spectrum displayed in Fig. 3 (c) in the whole energy and angular ranges. The shaded histogram shown in Fig. 3 (a) was accumulated by summing the local projection. The reconstructed  ${}^6\text{Be}$  spectrum, corrected for the instrumental efficiency and integrated over the whole angular range, is shown in Fig. 3 (b). The energy profiles predicted by theory for the  $0^+$ ,  $2^+$  and  $J^-$  states were found to be consistent with the experiment, and the ratios of reaction yields were determined for these states.

The resulting angular distributions for the  ${}^6\text{Be}$  states, as populated in the  ${}^1\text{H}({}^6\text{Li}, {}^6\text{Be})n$  reaction, are displayed in Fig. 6 (a). The angular distribution for the  ${}^6\text{Be}$  g.s. is in a good agreement with that obtained by using a  ${}^6\text{Li}(p, n)$  reaction [20] at a proton beam energy of 30.2 MeV, which yields a similar c.m. energy. The latter data were evaluated by using the missing-mass method, without applying any further data handling such as a complex efficiency corrections. The fact that the  $(p, n)$  results agree well with those obtained in our work is a strong confirmation of our data treatment. To calibrate the PWIA calculations we used the  ${}^6\text{Li}(p, n)$  data from Ref. [21]. The distributions of transferred momenta, measured for several incident proton energies, are well reproduced by using an  $r_0$  parameter of 0.33 fm [see the solid curve in Fig. 6 (b)]. Calculations with this  $r_0$  value also reproduce the peak positions of different components of the  ${}^6\text{Be}$  spectrum, obtained in our experiment [see Fig. 6 (a)].

The PWIA calculations indicate that the population of the  $0^+$  and  $2^+$  is associated mainly with  $\Delta L = 0$  and  $\Delta L = 2$  transitions, respectively. The  $2^+$  state also has an important  $\Delta L = 0$  contribution which is responsible for the rise of the cross section near the forward direction. The broad hump at  $E_T > 4$  MeV is apparently associated with  $\Delta L = 1$ . Qualitatively, the theoretical angular distributions are very similar to the experimental ones. However, they do not reproduce the tails of the measured distributions which extend to large c.m. angles. This deficiency is evidently connected to our simplified treatment of the reaction mechanism (PWIA), see discussion in Refs. [20, 22]. It is not expected that this deficiency affects the conclusions drawn from the correlation data. The evident correspondence of the measured angular distributions with  $\Delta L$  and the reasonable description of the experimental data by a simple PWIA calculation support, firstly, the dominance of the direct reaction mechanism in our experiment and, secondly, the overall consistency of the our data interpretation.

## 7. Major qualitative features of the IVSDM

To properly describe the two-body final state interactions within the framework of the three-body continuum remains a challenge for theoreticians. In view of the systematic disagreement between different calculations [23, 24, 25], it is evident that there is a serious problem in interpreting the soft E1 mode of two-neutron halo nuclei. In order to avoid this complexity we used a model for describing the soft responses which is simplified but presumably contains the major features of the relevant phenomena.

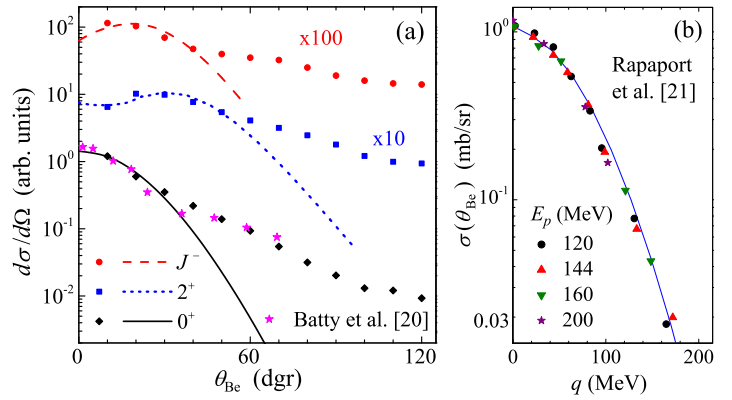


Fig. 6. (a) Angular distributions for states with different  $J^\pi$ . Symbols show the experimental data, and curves of the same color provide PWIA results. The  $0^+$  and  $2^+$  data are those obtained on resonance while the IVSDM  $J^-$  distribution is integrated over energy. The data of Ref. [20] for the  ${}^6\text{Be}$  g.s. are shown for comparison (pink stars). (b) Dependence of the g.s. cross-section on the transferred momentum calculated in PWIA (solid curve) and compared to the data obtained in Ref. [21] at different proton energies  $E_p$  (symbols).

Before discussing the IVSDM from a theoretical point of view, we emphasize several formal differences between the SDM and the IVSDM:

(a) In  $N = Z$  nuclei the E1 dipole transitions to states with the same isospin are strongly suppressed (e.g., by 3 orders of the magnitude) due to the small effective dipole charges of the nucleons. Therefore, the continuum population by  $\Delta T = 0$  transitions (like the SDM in  ${}^6\text{He}$ ) is not possible in  ${}^6\text{Li}$ .

(b) Electromagnetic isovector dipole transitions in  ${}^6\text{Li}$  (e.g. Ref. [26]) are induced by the spin-scalar operator, while in the strong isovector transitions the spin-vector part of the transition is expected to dominate. These operators correspond in Eq. (3) to the terms with coefficients  $\alpha$  and  $\beta$ , respectively, and populate distinctly different configurations in the final state.

(c) In  ${}^6\text{He}$ , the soft E1 transition to continuum is due to the interaction with the charged core *only*. In the case discussed here, the charge-exchange reaction occurs with the valence nucleons *only*. Therefore the IVSDM is expected to be sensitive to different nuclear-structure features than the SDM.

We consider the following qualitative features to be exclusive for our interpretation for the observed phenomenon:

(i) The proposed phenomenon represents a “major effect”. It can be seen in Fig. 3, that it is responsible for the major part, i.e. about 60%, of the charge-exchange cross-section populating the  ${}^6\text{Be}$  states up to  $E_T = 16$  MeV. It is a challenging task to try to interpret the dominant population of the non-resonant (negative parity) continuum, in comparison with the resonance continuum states.

(ii) The energy and angle dependence of the IVSDM cross-section depends on details of the reaction mechanism. In particular, in PWIA calculations it sizably depends on the transferred momentum  $q$ . Most likely, a qualitatively similar dependence exists in models for other reactions. This  $q$  dependence means that an attempt to characterize the IVSDM in terms of resonances with definite energies and widths does not take the underlying physics properly into account. The term “excitation mode” characterises this phenomenon correctly as it comprises a large observable effect which, how-

ever, is sensitive to the specific observation conditions.

(iii) The  ${}^6\text{Be}$  g.s. is particle-unstable and thus the strong population of the negative parity continuum can not be interpreted as being due to the soft excitations based on the weakly-bound and therefore radially-extended ground state. We interpret the observed phenomenon as having two roots, namely the radially extended g.s. of  ${}^6\text{Li}$  (not quite as large in  ${}^6\text{He}$ ) and the final state interactions in the negative parity continuum of  ${}^6\text{Be}$ .

(iv) The case of the IVSDM gives opportunity to test the concept of isobaric symmetry for this class of phenomena. According to the calculations shown in Fig. 4, the IVSDM is a “threshold-oriented” phenomenon. This means that the Coulomb effect can be observed as a dependence on *threshold energy*  $E_T$ , corresponding to a shift of the  ${}^6\text{Be}$  distributions to higher  $E_T$  values in comparison to the  ${}^6\text{He}$  data. However, the *excitation energies*  $E^*$  (counted from the respective ground states) of the peaks of the IVSDM distribution, are about the same for  ${}^6\text{He}$  and  ${}^6\text{Be}$  and maybe even somewhat lower for  ${}^6\text{Be}$ , which is quite unexpected.

## 8. Discussion of experiments related to the IVSDM

The standard compilation [27] including also the results obtained in charge-exchange reactions of the type  $(p, n)$  and  $({}^3\text{He}, t)$ , populating the  ${}^6\text{Be}$  continuum, yields an ambiguous situation concerning the data on the  ${}^6\text{Be}$  excitation energies  $E_T$  between 1.67 and 23 MeV. Older studies [28, 29, 5, and Refs. therein] were confined to narrow angular ranges. For certain angular ranges, excitation spectra similar to ours have been obtained [20, 5]. In all these cases, however, the spin-parity identification was not possible and excitations above the  $2^+$  state have generally been interpreted as being due to the three-body  $\alpha+p+p$  “phase volume”.

In Ref. [12], the  ${}^6\text{Be}$  spectrum was populated by using the  $(p, n)$  reaction at high proton energy, namely 186 MeV. Above the  $2^+$  state of  ${}^6\text{Be}$ , four groups of events with important  $\Delta L = 1$  components were distinguished, i.e. at  $E^* \sim 5.5$ , 10, 15, and 25 MeV. According to the interpretation given in Ref. [12], the cross section in the range  $E^* \sim 3 - 16$  MeV has a significant  $\Delta L = 0$  contribution, ranging from about 50% at  $E^* \sim 3$  MeV to zero at  $E^* \sim 12$  MeV, and an important quasi-free contribution, ranging from 20% at  $E^* \sim 3$  MeV to about 60% at  $E^* \sim 16$  MeV. This means that the total  $\Delta L = 1$  contribution is  $\sim 40\%$  on average in the whole  $E^*$  interval from 3 to 16 MeV. In contrast, we do not observe separate groups of events in this energy range where our spectrum is very smooth. As our experiment is characterized by good energy resolution and has excellent statistics, possible structures can not be masked by instrumental problems. Our data exclude any sizable contribution of  $\Delta L = 0$  transfer and/or of uncorrelated background in this energy range.

There is a major difference between Ref. [12] and our work in the interpretation of experimental results. In Ref. [12] the structures at  $E^* \sim 5.5$ , 10, 15 MeV in  ${}^6\text{Be}$  were considered as evidence for important qualitative phenomena occurring in light nuclei and were interpreted as the low-energy “off-springs” of the giant-dipole and giant spin-dipole resonance. Our observation of the single smooth structure in the  $E^*$  range between 3 and 15 MeV favours of the IVSDM interpretation. Though the IVSDM has the same transition

quantum numbers as dipole and spin-dipole resonances, it is not a resonance but a *continuum mode*, and is not a collective but a *cluster phenomenon*.

The isovector dipole strength has been considered in the studies of “mirror”  ${}^6\text{Li}({}^A\text{Z}, {}^A\text{Z} + 1){}^6\text{He}$  reactions [9, 30, 10, 11]. The most recent works [10, 11] provide good-quality data and sophisticated interpretations. Our theoretical results indicate very similar behavior for the IVSDM populating the continuum of  ${}^6\text{He}$  and  ${}^6\text{Be}$ . This enables us to speculate about the IVSDM in  ${}^6\text{He}$  by using our  ${}^6\text{Be}$  data together with considerations concerning the isobaric symmetry. We suggest an entirely different interpretation for the  ${}^6\text{He}$  data obtained in Refs. [10, 11], which is based on the following considerations:

(I) According to Ref. [10], the broad structure at  $E^* = 4 - 15$  MeV consists of, firstly, the “dipole excitation mode” at  $\sim 4$  MeV with  $\Delta S = 1$ , secondly, the “low-energy wing” of the GDR at  $\sim 8.5$  MeV formed by a  $\Delta S = 0$  transition, and, thirdly, the “spin dipole resonance” at  $\sim 8.5$  MeV with  $\Delta S = 1$  which was assumed to have the same profile as the GDR. This work used  $\gamma$ -ray coincidences to distinguish the  $\Delta S = 0, 1$  contributions. However, the measurements were confined to extreme forward angles ( $\sim 2^\circ$ ), which makes the separation of contributions with different  $\Delta L$  a difficult task. The conclusion of Ref. [10] that the “dipole excitation mode” peak has higher energy than that obtained previously for SDM in Refs. [4, 24] can easily be explained by comparing the SDM and IVSDM spectra predicted in our work, see Fig. 4. We are unable to separate the “dipole excitation mode” and the “spin dipole resonance”, as defined in Ref. [10]), in our experiment which does not have any specific reaction-mechanism or quantum-number selectivity with that respect. However, our model calculation is able to reproduce the low-energy peak observed in the electromagnetic transition [4] [see Fig. 7 (a)] and the broad cross-section distribution obtained in the charge-exchange transition [10] [see Fig. 7 (b)]. Therefore, we suggest to interpret the continuum obtained in Ref. [10] in a range of 4 – 15 MeV of  ${}^6\text{He}$  excitation as being due the same IVSDM phenomenon as the one proposed in the present work.

(II) According to Ref. [11], two broad structures were populated by  $\Delta L = 1$  transfer in the  ${}^6\text{Li}({}^3\text{He}){}^6\text{He}$  reaction, namely one at  $E^* \sim 5$  MeV, decomposed into 4.4, 7.7, and 9.9 MeV peaks, and another one at  $E^* \sim 15$  MeV. Within the interpretation given in Ref. [11], the underlying reaction mechanism is “semi-phenomenological parameterisation of quasi-free scattering”, contributing more than 50% at  $E^* \sim 10$  MeV. The  $E^* \sim 5$  MeV structure is interpreted as being composed of intruder states, which indicates quenching of the  $1p-2s$  shell gap in  ${}^6\text{He}$ . In our work, the correlation patterns displayed in Fig. 5 exclude the possibility of any sizable phase-volume-like “background”. The simple dynamic mechanism of the IVSDM population described by Eqs. (3) and (4) does not require intruder states as the  $s$ -wave motion in the system is non-resonant, and thus does not imply any shell gap quenching.

In our experiment we obtained not only the energy profile of the  ${}^6\text{Be}$  spectrum but also the complete set of kinematic variables. We observe a systematic structure-less behavior of all variables with energy  $E_T$  at a high confidence level, and do not see any reason for decomposing the continuum into components. We treat the continuum up to  $E_T \sim 16$  MeV

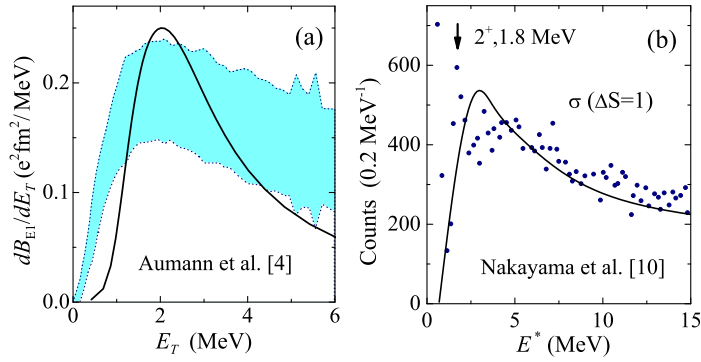


Fig. 7. Qualitative comparison (a) of SDM calculations (solid curve) with  ${}^6\text{He}$  data [4] (blue shaded range), and (b) IVSDM calculations (solid curve) with  ${}^6\text{He}$  data [10] (diamonds).

(at least the most part of the corresponding cross section) as being due to one and the same phenomenon, namely the IVSDM.

Concluding this discussion, our interpretation is different from that presented in Refs. [12, 10, 11], and can significantly clarify the situation concerning the “soft” excitations in  $A = 6$  nuclei. As can be seen from Figs. 3 and 7, our approach provides a consistent explanation of the three different sets of data, namely the SDM in  ${}^6\text{He}$  and the IVSDM in  ${}^6\text{He}$  and in  ${}^6\text{Be}$ .

## 9. Conclusion

Accurate data on the three-body  $\alpha + p + p$  continuum of  ${}^6\text{Be}$  system were obtained in the charge-exchange  $p({}^6\text{Li}, {}^6\text{Be})n$  reaction. The  ${}^6\text{Be}$  spectrum up to  $E_T = 16$  MeV is well described by assuming the population of three main structures in  ${}^6\text{Be}$ , i.e. the  $0^+$  state at 1.37 MeV, the  $2^+$  state at 3.05 MeV, and a mixture of  $\{0^-, 1^-, 2^-\}$  continuum in the  $E_T$  range from 4 to 16 MeV. The negative-parity continuum is interpreted as a novel phenomenon, the IVSDM which may offer new opportunities in the nuclear structure studies.

*Acknowledgments.* — The authors are grateful to Profs. Yu.Ts. Oganessian and S.N. Dmitriev for continuous support of this experiment. The authors are indebted to Prof. E. Roeckl for careful reading of the manuscript and numerous improvements. This work was supported by the Russian Foundation for Basic Research grant RFBR 11-02-00657-a. L.V.G. is supported by FAIR-Russia Research Center grant, the Helmholtz International Center for FAIR within the LOEWE program by the State of Hessen (Germany), and Russian Ministry of Education and Science grant NSH-7235.2010.2.

## REFERENCES

1. K. Ikeda, INS Report JHP-7, in Japanese (1988).
2. P. Hansen, B. Jonson, *Europhys. Lett.* **4** (1987) 409.
3. C. Bertulani, G. Baur, *Nucl. Phys.* **A480** (1988) 615.
4. T. Aumann, *Eur. Phys. J. A* **26** (2005) 441.
5. O.V. Bochkarev *et al.*, *Sov. J. Nucl. Phys.* **55** (1992) 955.
6. V.I. Goldansky, *Nucl. Phys.* **19** (1960) 482.
7. L.V. Grigorenko *et al.*, *Phys. Lett.* **B677** (2009) 30.
8. L.V. Grigorenko *et al.*, *Phys. Rev. C* **80** (2009) 034602.
9. S. Sakuta *et al.*, *Europhys. Lett.* **22** (1993) 511.
10. S. Nakayama *et al.*, *Phys. Rev. Lett.* **85** (2000) 262.
11. T. Nakamura, *Eur. Phys. J. A* **13** (2002) 33.

12. X. Yang *et al.*, *Phys. Rev. C* **52** (1995) 2535.
13. <http://flerovlab.jinr.ru/flnr/u400m.html>
14. A.M. Rodin *et al.*, *Nucl. Instr. Meth.* **A391** (1997) 228.
15. B. Danilin *et al.*, *Phys. Rev. C* **43** (1991) 2835.
16. L.V. Grigorenko, K. Langanke, N.B. Shul'gina, M.V. Zhukov, *Phys. Lett.* **B641** (2006) 254.
17. M.S. Golovkov *et al.*, *Phys. Lett.* **B672** (2009) 22.
18. H. Esbensen, G.F. Bertsch, *Nucl. Phys.* **A542** (1992) 310.
19. M. Pfützner, L.V. Grigorenko, M. Karny, K. Riisager, arXiv:1111.0482, *Rev. Mod. Phys.* in print.
20. C. Batty *et al.*, *Nucl. Phys.* **A120** (1968) 297.
21. J. Rapaport *et al.*, *Phys. Rev. C* **41** (1990) 1920.
22. F. Petrovich *et al.*, *Nucl. Phys.* **A563** (1993) 387.
23. A. Cobis, D. Fedorov, A. Jensen, *Phys. Rev. Lett.* **79** (1997) 2411.
24. B. Danilin, I. Thompson, J. Vaagen, M. Zhukov, *Nucl. Phys.* **A632** (1998) 383.
25. T. Myo, K. Kato, S. Aoyama, K. Ikeda, *Phys. Rev. C* **63** (2001) 054313.
26. B.L. Berman, S.C. Fultz, *Rev. Mod. Phys.* **47** (1975) 713.
27. D. Tilley *et al.*, *Nucl. Phys.* **A708** (2002) 3.
28. R. Givens, M. Brussel, A. Yavin, *Nucl. Phys.* **A187** (1972) 490.
29. D.F. Geesaman *et al.*, *Phys. Rev. C* **15** (1977) 1835.
30. J. Jänecke *et al.*, *Phys. Rev. C* **54** (1996) 1070.